

1 Dynamical Cross-Correlated Physics Project

– Quantum-beam studies on dynamical cross-correlated physics in strongly-correlated-electron systems –

Project Leader: Hajime Sagayama

Owing to strong interelectron interactions, spin, orbital occupancy, orbital angular momentum, charge, and lattice act as degrees of freedom, and consequently, their cross-correlation dominates physical phenomena in strongly correlated electron systems. When more than one of them are simultaneously in order, such cross-correlations cause a non-conjugated external field response such as a magnetization change by applying an electric field, thereby producing advanced features in a monolithic device. The objective of this project is to clarify the mechanism of the huge cross-correlation properties of strongly correlated systems in a microscopic point of view. In this work, we report two studies in progress as follows.

1-1 Microscopic mechanism of room-temperature colossal magnetoresistance in double-perovskite manganite [1]

Colossal magnetoresistance (CMR) in a series of perovskite manganites $RE_{1-x}AE_xMnO_3$ (where RE is a trivalent rare earth and AE a divalent alkaline earth metal) has attracted much attention for decades [2]. These drastic phenomena are caused by the strong coupling among charge, orbital, and spin degrees of freedom. The negative magnetoresistance phenomena in perovskite manganites are classified into two categories. A rather gradual and moderate negative magnetoresistance (MR) was observed around room temperature in $La_{1-x}Sr_xMnO_3$ [3, 4]. This reduction is attributed to the gradual increase in the band width by aligning the Mn spins in a magnetic field. Another type of CMR effect, which is caused by the melting of charge ordering, was discovered in

many compounds like $Pr_{1-x}Ca_xMnO_3$ [5, 6]. The charge-order melting type CMR is much larger and steeper than that the former type. Although the magnetic field necessary for a one-order decrease in resistivity is about 0.2 T [7], the melting type CMR has been rarely observed at room temperature to date because the transition temperature of the charge ordering is lower than the room temperature in most cases.

We recently succeeded in achieving single-crystal growth of an A-site ordered perovskite manganite $NdBaMn_2O_6$ by a floating zone method and observed a first-order metal-insulator phase transition that was not accompanied by any magnetic ordering [8]. A high-quality single crystal exhibits the metal-insulator transition near 300 K. In a magnetic field, the phase transition temperature decreases as shown in Figs.2(e) and (f). Therefore, the insulating phase changes to the metallic phase on the application of a magnetic field approximately at room temperature. The value of resistivity change exceeds two orders of magnitude.

Charge and orbital arrangement in the insulat-

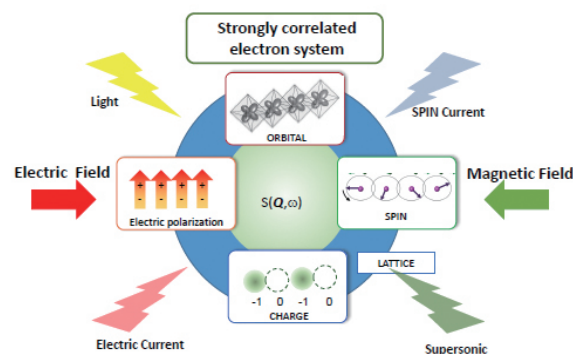


Fig. 1: Schematic view of the cross-correlation among multi-degrees of freedom, spin, electric polarization, charge, orbital, and lattice in a strongly correlated electron system.

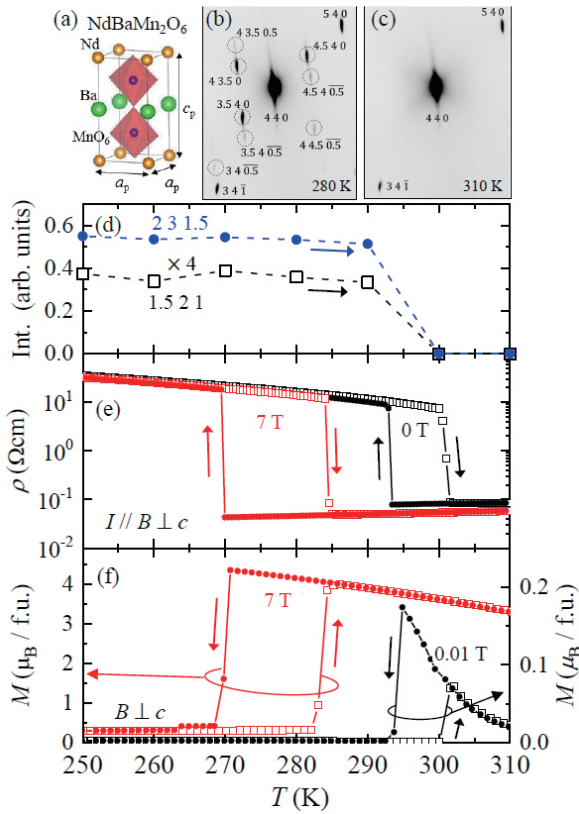


Fig. 2: X-ray oscillation photographs of a NdBaMn₂O₆ single crystal approximately (4 4 0) at (b) 280 K and (c) 310 K. Temperature dependence of (d) integrated intensities of (2 3 1.5) and (1.5 2 1) super reflections, (e) electrical resistivity at 0 T, and 7 T, and (f) magnetization at 0.01 T and 7 T. These figures are referred from [1].

ing phase were supposed to be ferro-ordering of Mn^{3.5+} and x²-y² orbital, respectively [8]. However, this scenario cannot explain the in-plane insulative resistivity. To clarify the microscopic mechanism of the M-I transition, we performed a single-crystal x-ray diffraction experiment on BL-8B at the Photon Factory, KEK. Only the fundamental reflections of the $\sqrt{2}a_p \times \sqrt{2}a_p \times c_p$ unit cell were observed above T_{MI} , as reported previously. In contrast, many superlattice reflections with a propagation vector of (1/2 0 1/2) or (0 1/2 1/2) appear below T_{MI} , as shown in Fig. 2(b). All the x-ray reflections in this work are indexed based on the $\sqrt{2}a_p \times \sqrt{2}a_p \times c_p$ unit cell, where a_p and c_p are lattice constants of the simple tetragonal perovskite unit cell illustrated in Fig. 2(a). The superlattice reflections are more than six orders weaker than some fundamental reflections. The results indicate that the unit cell below T_{MI} is $2\sqrt{2}a_p \times \sqrt{2}a_p \times 2c_p$. It is similar to the charge ordering phase of another A-site ordered perovskite manganite, SmBaMn₂O₆, between 200 K and 380 K, suggest-

ing that the charge and orbital ordering patterns of these materials are identical, as illustrated in Fig. 3(b) [9]. On the other hand, our studies using neutron diffraction indicate that Mn moments are aligned to form simple A-type antiferromagnetic order, which is evidently inconsistent with the checkerboard-type charge ordering. To unravel this contradiction, further x-ray and neutron diffraction studies are in progress in this project.

1-2 Observation of electromagnetic fluctuations in multiferroic material MnWO₄

Static magnetoelectric couplings in multiferroic materials are currently being unraveled, while their dynamic magnetoelectric nature is still a matter of further study. Collective magnetic-electric excitations have been intensively investigated as “electromagnons” in the ordered state [10]. For application to electronic devices, critical electromagnetic fluctuations should also be studied around the transition temperature, where the magnet-electric susceptibility is expected to be strongly enhanced. MnWO₄ is a canonical example of a multiferroic where ferroelectricity is driven by a cycloidal-spin-spiral order [11,12]. It crystallizes in a monoclinic crystal structure, where Mn²⁺ ions are interconnected via the common edges of distorted MnO₆ octahedra (Fig. 4(a)) [13]. On cooling, MnWO₄ exhibits successive magnetic phase transitions at 13.5 K (T_{N3}), 12.7 K (T_{N2}), and

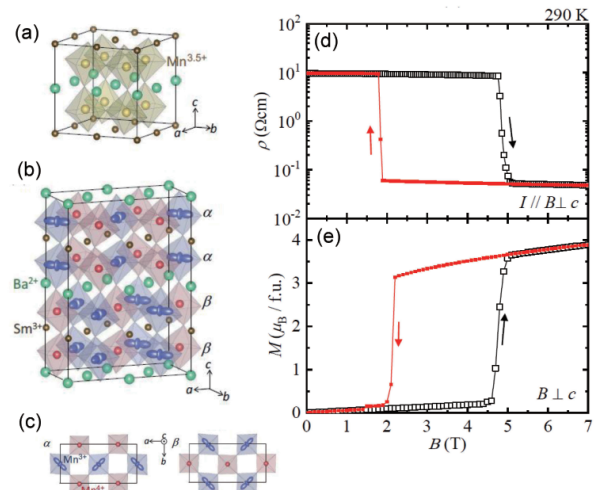


Fig. 3: Predicted charge and orbital arrangement (a) above T_{MI} and (b) below T_{MI} . (c) Two types of charge and orbital arrangements in the ab plane. Figs. (a), (b), and (c) are referred from [13]. (d) Magnetic field dependence of resistivity and magnetization at 290 K [1].

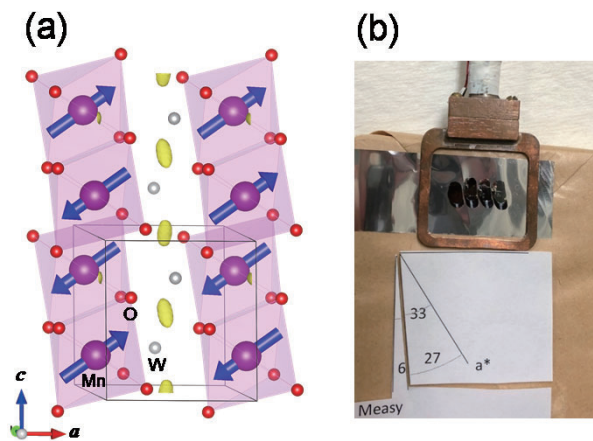


Fig. 4: (a) Illustration of the collinear spin configuration of MnWO_4 in the AF1 phase. Yellow lobes represent the potential minima. Solid lines highlight the monoclinic unit cell. (b) Alignment of the single crystals on the sample rod.

7.6 K (T_{N1}) [14]. Corresponding magnetic structures of the respective phases are a sinusoidally modulated collinear antiferromagnetic structure (AF3, $T_{N2} < T < T_{N3}$) with wave vector $\mathbf{k} = (-0.214 \ 1/2 \ 0.457)$, an incommensurate spiral structure (AF2, $T_{N1} < T < T_{N2}$), and a commensurate collinear structure (AF1, $T < T_{N1}$) with $\mathbf{k} = (-1/4 \ 1/2 \ 1/2)$. Spontaneous electric polarization $P//b$ has only been observed in the AF2 phase through the inverse Dzyaloshinskii–Moriya mechanism [15,16].

Complex permittivity measurement suggests critical decrease in speed of the corresponding magnetolectric fluctuations in 10 MHz ~ 1 GHz order in MnWO_4 , which resembles a soft-mode behavior in canonical ferroelectrics [17]. Microscopic investigations in this frequency range are required to clarify the magnetolectric dynamics. In this work, we have studied such electromagnetic fluctuations in MnWO_4 using the muon spin rotation/relaxation (μSR) technique around the transition temperatures, T_{N2} and T_{N3} .

Single crystals of MnWO_4 were grown by the floating-zone method. The experiments were conducted at TRIUMF using Lampf on M20 beamline and NuTime on M15 beamline. The pulsed muon facility in J-PARC (ARTEMIS on S1 beamline) was also used to obtain data in a long-time window. The incident direction of muon beam is parallel to the b axis (Fig. 4(b)).

Figure 5(a) displays a selected zero-field (ZF) μSR time spectra at several temperatures. Below T_{N3} , the spectra show rapid decay, which scale with an evolution of an internal local magnetic

field. As shown in Fig. 5(b), clear spontaneous oscillations are only observed in the early time region in the AF1 phase ($t < 0.2 \ \mu\text{s}$), reflecting a large local field of the commensurate collinear spin structure. As inferred from the FFT spectra, some frequency peaks were identified, indicating that MnWO_4 possesses several magnetically-inequivalent muon stopping sites. The obtained spectra were reproduced well by the following equation,

$$A(t) = A_T \sum_i^n f_i \cos(\omega_i t + \phi_i) \exp(-\lambda_{Ti} t)^\beta + A_L \exp(-\lambda_L t), \quad (1)$$

where A_T (A_L) is the positron decay initial asymmetry of the transverse (longitudinal) components, and f_i , ω_i , and ϕ_i are the fractional yield, precession frequency, and initial phase of transverse components, respectively. λ_T (λ_L) represents the relaxation rate of the transverse (longitudinal) component and the power β is the additional parameter. For the analysis of the pulsed muon data of J-PARC, Eq. (1) should be simplified to the following relaxation equation because of the limited time resolution (~ 100 ns) of the pulsed muon source,

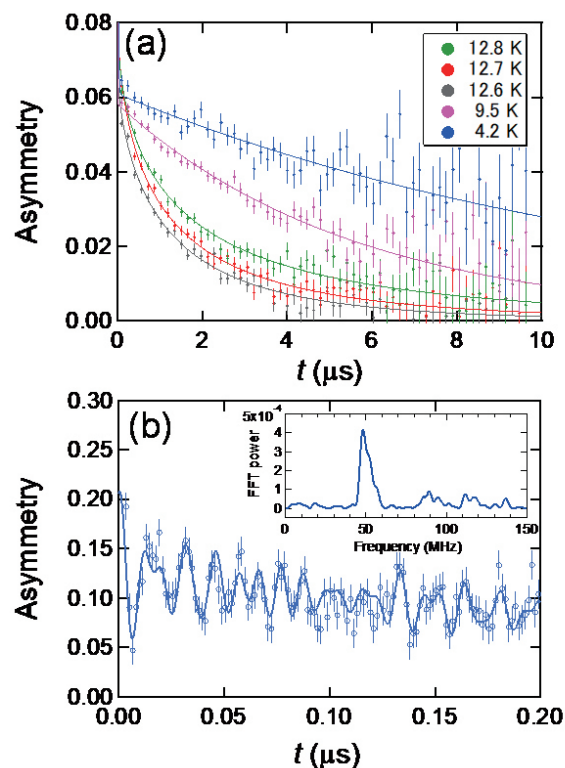


Fig. 5: (a) Selected zero-field μSR time spectra taken below T_{N3} . (b) Early time parts of the spectrum at 4.2 K. Inset shows Fast Fourier transform (FFT) spectrum at 4.2 K under zero magnetic field.

$$A(t) = A_T \exp(-\lambda'_T t) + A_L \exp(-\lambda_L t) + A_{BG}, \quad (2)$$

where λ'_T is the averaged Gaussian relaxation rate of the transverse relaxation component and A_{BG} is a constant background contribution from those muons that stop in the sample holder or cryostat tail.

Figure 6(a) shows the temperature dependence of λ_L under zero external field. On cooling, λ_L exhibits the typical sharp peak at T_{N3} owing to the critical decrease in speed of Mn spin fluctuation near the paramagnetic-antiferromagnetic transition. On cooling further, it shows a moderately broad peak at T_{N2} that is apparently different from the generic second-order transition.

In the extreme motional narrowing limit, a spin fluctuation rate ν is deduced using the Redfield model for a longitudinal relaxation rate λ_L under an effective field ($B_{\text{eff}} = B_0 + B_{\text{local}}$, B_0 is the external field) [18],

$$\lambda_L \approx \frac{2\delta^2\nu}{\nu^2 + \gamma_\mu^2 B_{\text{eff}}^2}. \quad (3)$$

If $\gamma_\mu B_{\text{eff}} (= \omega_{\text{eff}}) \gg \nu$, where magnetic orders set in at higher temperatures, λ_L is approximately proportional to $1/\omega_{\text{eff}}^2$ as $\lambda_L = 2\delta^2\nu / \omega_{\text{eff}}^2$. Assuming that the precession frequency ω_{eff} practically corresponds to the transverse relaxation rate λ'_T in Eq.2, we obtained the T-dependence of ν together

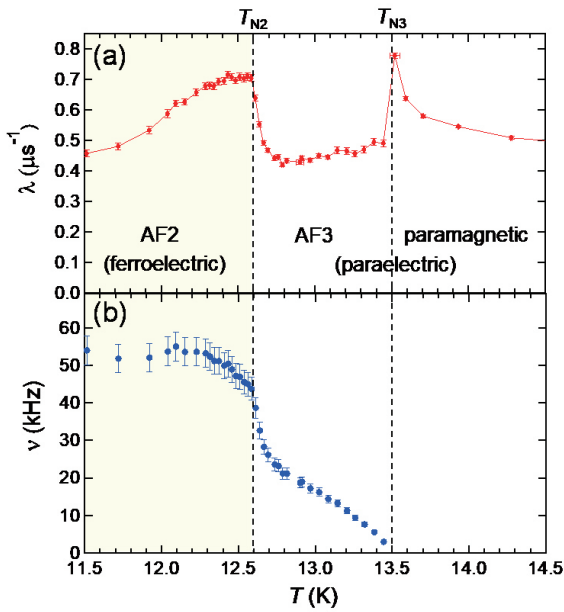


Fig. 6: Comparison between the temperature dependence of (a) the longitudinal relaxation rate λ and (b) the spin fluctuation rate ν around the ferroelectric transition at T_{N2} .

with λ_L , as shown in Fig. 6(b).

Below T_{N3} , ν gradually increases with a decrease in temperature. As the temperature approaches T_{N2} , the increase rate of ν increases, and then gradually decreases, emerging as a small kink at T_{N2} . This behavior is quite different from that of ordinary magnetic transition accompanying a divergence of spin fluctuation. This may be due to a strong coupling between the magnetic fluctuation and the polar lattice distortion in multiferroics. The slow ν is partly justified because a characteristic minimum in the real part of dielectric permittivity $\epsilon'(t)$ can be taken as fingerprint for a critical decrease in speed [8]. The slow spin dynamics in the AF2 phase may be attributed to the first-order nature of the ferroelectric phase transition. We are now planning detailed measurements of the dielectric permittivity in the low-frequency range (< 1 MHz) to elucidate the close relationship between magnetic and electric fluctuation in MnWO_4 .

References

- [1] S. Yamada, N. Abe, H. Sagayama, K. Ogasawara, T. Yamagami, and T. Arima, Phys. Rev. Lett. in press.
- [2] Y. Tokura and Y. Tomioka, J. Magn. Magn. Mater **200**, 1 (1999).
- [3] Y. Tokura, A. Urushibara, Y. Moritomo, T. Arima, A. Asamitsu, G. Kido, and N. Furukawa, J. Phys. Soc. Jpn. **63**, 3931 (1994).
- [4] A. Urushibara, Y. Moritomo, T. Arima, A. Asamitsu, G. Kido, and Y. Tokura, Phys. Rev. B **51**, 14103 (1995).
- [5] Y. Tomioka, A. Asamitsu, Y. Moritomo, and Y. Tokura, J. Phys. Soc. Jpn. **64**, 3626 (1995).
- [6] Y. Tomioka, A. Asamitsu, H. Kuwahara, Y. Moritomo, and Y. Tokura, Phys. Rev. B **53**, R1689 (1996).
- [7] H. Kuwahara, Y. Moritomo, Y. Tomioka, A. Asamitsu, M. Kasai, R. Kumai and Y. Tokura, Phys. Rev. B **56**, 9386 (1997).
- [8] S. Yamada, H. Sagayama, K. Higuchi, T. Sasaki, K. Sugimoto, and T. Arima, Phys. Rev. B **95**, 035101 (2017).
- [9] H. Sagayama, S. Toyoda, K. Sugimoto, Y. Maeda, S. Yamada, and T. Arima, Phys. Rev. B **90**, R241113 (2014).
- [10] Y. Tokura and N. Kida, Phil. Trans. R. Soc. A **369**, 3679 (2011).
- [11] K. Taniguchi, N. Abe, T. Takenobu, Y. Iwasa,

- and T. Arima, Phys. Rev. Lett. **97**, 097203 (2006).
- [12] A. H. Arkenbout, T. T. M. Palstra, T. Siegrist, and T. Kimura, Phys. Rev. B **74**, 184431 (2006).
- [13] H. Dachs, H. Weitzel, and E. Stoll, Solid State Commun. **4**, 473 (1966).
- [14] G. Lautenschläger, H. Weitzel, T. Vogt, R. Hock, A. Böhm, M. Bonnet, and H. Fuess, Phys. Rev. B **48**, 6087 (1993).
- [15] H. Katsura, N. Nagaosa, and A. V. Balatsky, Phys. Rev. Lett. **95**, 057205 (2005).
- [16] I. A. Sergienko and E. Dagotto, Phys. Rev. B **73**, 094434 (2006).
- [17] D. Niermann, C. P. Grams, P. Becker, L. Bohatý, H. Schenck, and J. Hemberger, Phys. Rev. Lett. **114**, 037204 (2015).
- [18] A. Yaouanc and P. Dalmasde Réotier, Muon Spin Rotation, Relaxation and Resonance: Applications to Condensed Matter, Oxford University Press, Oxford, (2011).